International Journal of Recent Technology and Applied Science
p-ISSN: 2721-2017, e-ISSN: 2721-7280

Original Research Paper

Effect of Defect Geometry and Strain Rate on Mechanoelectrochemical Behavior of X100 Steel Pipelines

Muhammad Zacky Syah[1], Andoko Andoko[1*], Riduwan Prasetya[1]

[1] *Department of Mechanical and Industrial Engineering, Faculty of Engineering, State University of Malang. Indonesia.*

Article History
Received:
13.12.2024

Revised:
21.01.2025

Accepted:
07.02.2025

***Corresponding Author:**
Andoko Andoko
Email:
andoko.ft@um.ac.id

Abstract: Corrosion and mechanical issues in high-strength X100 steel pipelines present major difficulties for the safety and dependability of energy transport systems. This research investigates the joint impacts of defect shape and strain rate on stress distribution as well as electrochemical behavior through COMSOL Multiphysics simulations. Findings show that defects with elevated aspect ratios generate intense stress gradients, resulting in focused plastic deformation and the onset of cracks. Additionally, higher strain rates worsen stress concentration and speed up anodic and cathodic reactions, amplifying hydrogen embrittlement and the deterioration of materials. As time passes, the redistribution of stress due to degradation leads to structural instability and increases the likelihood of failure. These results highlight the significance of combining mechanical and electrochemical analyses to gain a deeper insight into degradation mechanisms. This research offers important perspectives for enhancing defect surveillance, refining cathodic protection methods, and guaranteeing the enduring reliability of pipelines in dynamic and corrosive settings.

Keywords: Defect Geometry, Mechanoelectrochemical Behavior, Pipeline Corrosion, Strain Rate Effects, X100 Steel.

1. Introduction

High-strength steel pipe is an essential component in oil and gas transportation, which faces mechanical stress and corrosive environments simultaneously. X100 steel has become a top choice due to its of high tensile strength, outstanding ductility and corrosion resistance, making it superior to materials such as X70 steel [1]. Its granular microstructure consisting of bainite and ferrite provides stability in the face of high internal stresses [2]. However, the material remains susceptible to localised corrosion that can lead to structural failure. This integrity challenge is increasingly relevant with the increasing industrial need for more efficient and safe pipelines.

Despite the benefits of cathodic protection systems, they often weaken in certain areas, particularly around complex defect geometries. This creates unprotected zones, significantly increasing the risk of localized corrosion [3]. Moreover, the interplay between stress distribution, current density, and corrosion potential is critical for ensuring pipeline reliability under high operating pressures [4]. For example, defects with high aspect ratios have been shown to generate stress concentrations nearing the material's yield strength, potentially triggering localized plastic deformation [5]. These issues are further exacerbated by increased anodic current density within the deepest zones of defects, which accelerates localized corrosion rates [6]. While these findings provide valuable insights, a comprehensive framework that integrates defect geometry variables with strain rates remains scarce. This highlights the need for a novel approach that combines mechanical and electrochemical simulations to evaluate the combined effects of these critical variables.

This research proposes a COMSOL Multiphysics simulation-based approach to comprehensively integrate mechanical and electro-chemical analyses. This approach explores the relationship between the variables of defect geometry and strain rate on maximum stress distribution, anodic current density, and cathodic protection effectiveness. The advantage of this method is its ability to simulate the real conditions of an X100 steel pipeline, thus providing an in-depth insight into the damage potential of the material. In addition, the method enables the evaluation of cathodic protection effectiveness on complex defect geometries, offering guidance for the development of more effective mitigation strategies. This approach is expected to improve pipeline reliability and safety, and extend the service life of pipeline systems under various operational conditions.

This study aims to evaluate the effect of the variable combination of defect geometry and strain rate on stress distribution, corrosion rate, and cathodic protection effectiveness in X100 steel. COMSOL-based numerical simulations were used to model the mechanical and electro-chemical interactions in the pipeline with elliptical-shaped defects. The results of this study make a significant contribution to understanding the dynamics of defect growth and the limits of cathodic protection effectiveness. By providing data-driven guidance for safer pipeline design, this research can support the reduction of material failure risk and improvement of operational efficiency in the oil and gas industry.

2. Literature Review

2.1. Mechanoelectrochemical Theory

The mechanoelectrochemical (M-E) theory addresses the relationship between mechanical stress and electrochemical reactions, which can help explain how corrosion affects steel pipes. The theory encompasses the concept of electrochemical reaction kinetics and investigates how stress and strain affect pipeline materials in dynamic operational circumstances [7]. Mechanoelectrochemical interactions may speed up the degradation process and exacerbate corrosion defects in pipeline materials [8]. To investigate this phenomena, finite element (FE) model-based approaches have been frequently employed to simulate M-E interactions. This approach provides for a complete examination of the impact of defect shape, internal stresses, and stress distribution on corrosion progression.

2.2. Stress-Corrosion Cracking

Stress-Corrosion Cracking (SCC) is one of the corrosion-related mechanisms that can cause serious damage to high-strength steel pipelines. SCC occurs as a result of mechanical stress combined by a corrosive environment [9]. Corrosion occurs on the pipe surface when subjected to high operational pressures and extreme conditions such as seawater or sour gas [10] [11]. As a result, there is a continuous need for regular monitoring, corrosion prevention, and designs that reduce material stress in order to avoid SCC.

2.3. Fracture Mechanics and Crack Propagation

The principles of crack mechanics try to explain how cracks occur and propagate [12]. When a liquid or gas stresses a pipe from the inside, the tension is centred at the tip of a preexisting small crack [13]. Crack mechanics relies on two major ideas such as: the stress intensity factor (K) and strain energy (G) [14] [15]. The stress intensity factor indicates how much stress exists around the crack tip. Strain energy, on the other hand, refers to the energy released as the fracture grows bigger. When the energy surpasses a certain limit, the crack will expand and spread [16].

2.4. Electrochemical Corrosion Mechanisms

Steel pipes possess various kinds of corrosion mechanisms, including pitting corrosion, erosion corrosion, uniform corrosion, and intergranular corrosion. Pitting corrosion occurs when the steel undergoes corrosion in a concentrated area, resulting in small, deep pits [17]. Erosion corrosion appears when the steel coating becomes eroded by friction or the flow of a highly opposed liquid [18]. Uniform corrosion happens when the surface area decreases uniformly as a result of chemical reactions with the environment [19]. Intergranular corrosion occurs between steel granules and usually happens to an insufficient or excess of an element that decreases the steel's resistance to corrosion [16].

2.5. Tafel Law and Corrosion Kinetics

In simple terms, Tafel's law states that as the voltage increases, correspondingly increases the corrosion rate, and inversely [20]. This law determines the corrosion rate by measuring the change in electrode potential during the corrosion process. Tafel curve analysis can help identify important electrochemical characteristics like corrosion potential and Tafel coefficient.

2.6. Hydrogen Embrittlement

Hydrogen embrittlement happens when steel becomes brittle due to the absorption of hydrogen atoms [21]. Very small hydrogen atoms can enter the metal and reduce the tension necessary for formation and extend the crack, creating embrittlement. This is quite common in steel and alloys [22]. Hydrogen embrittlement can generate cracks as a result of applied mechanical or residual stresses.

2.7. Finite Element Method for Stress and Corrosion Analysis

The finite element technique (FEM) is used to study stress distribution and corrosion in pipelines by splitting apart the pipeline structure into individual pieces for easier analysis. Each element has unique mechanical and electrical properties. Various boundary conditions can be set based on preference, such as internal pressure, temperature, and external contaminants, in order to predict how these will effect the stress distribution and corrosion rate of the pipeline [23] [24]. The method allows precise simulations of actual conditions, allowing for the development of preventative measures and ensuring the pipeline's structural integrity in the long run.

2.8. Defect Geometry and Stress Concentration

The geometry of the pipeline defect has a significant impact on the stress distribution and concentration surrounding itself. Defects with severe geometries, such as fractures or microscopic indentations, can create extremely high stress concentrations along the defect's edges, also known as "stress concentration". This focused stress can accelerate crack initiation and propagation [25]. On the other hand, faults with smoother, more rounded shapes, such as wide or curved indentations, tend to distribute stress more uniformly and lessen the effect of stress concentration.

2.9. Electrochemical Impedance Spectroscopy

Electrochemical Impedance Spectroscopy (EIS) is a valuable instrument for evaluating electrochemical behaviour on pipelines as it measures the system's impedance across a wide frequency range. This method assists in understanding corrosion processes, coating degradation, and the overall integrity of pipeline materials. EIS generates a Nyquist plot by applying a tiny AC voltage and measuring the current, which offers data on the pipeline surface's resistive and capacitive behaviour. This information is essential for estimating pipeline longevity, optimising maintenance schedules, and creating corrosion prevention strategies1. EIS is a non-destructive technology, making it a useful instrument for continuous monitoring and maintaining the safety of pipelines.

2.10. Cathodic Protection Theory

Cathodic protection protects the pipeline against corrosion through rendering it the cathode in an electrochemical cell. The concept is to connect the pipeline to a more reactive material, like a sacrificial anode (e.g., magnesium, zinc, or aluminium), which is more easily oxidised. In this technique, the sacrificial anode will corrode while the pipeline is protected. Alternatively, an electric current from an external source can be used to deliver a protective current to the pipeline, preventing oxidation. Nevertheless, cathodic protection has some limits, particularly in places with severe defect geometry [26]. Sharp defects can result in large stress concentrations, increasing the probability of cracking and localised corrosion. The distribution of protective current in certain regions may be unequal, leaving some segments of the pipeline vulnerable to corrosion [27]. As a result, in addition to cathodic protection, coating and annual inspections are required to maintain the pipeline's structural integrity.

2.11. Material Behavior under Cyclic Loading

Cyclic loading and high strain rate have a major effect on X100 steel's mechanical properties. Under cyclic loading, X100 steel loses tensile strength and toughness due to damage produced by repetitive load cycles [28]. High strain rates, on the other hand, boost X100 steel's tensile strength due to the rapid elastic response to the applied load. However, a high strain rate might produce internal wear, resulting in early collapse. As a result, an in-depth understanding of the relationship between cyclic loading and strain rate is required to assure the structural integrity of X100 steel in a variety of industrial applications.

2.12. Interaction of Electrochemical and Mechanical Variables

The interaction of electrochemical and mechanical variables may accelerate pipeline degradation due to the synergistic effect of mechanical stress and corrosion. Excessive mechanical stress can generate micro-cracks on the pipeline surface, allowing corrosive substances to enter the system [29]. Electrochemical corrosion accelerates damage to these regions, weakening the pipeline structure and increasing the probability of failure. Repeated loading cycles can also cause cracks to spread more quickly. More reliable pipeline design requires a mix of cathodic protection, good coatings, and regular monitoring to detect early damage.

3. Methodology

3.1. Initial and Boundary Geometrical Parameters

The FE simulation of the mechanoelectrochemical effect on X100 steel pipeline corrosion was performed using COMSOL Multiphysics. The pipeline model consisted of a steel segment with a wall thickness of 19.1 mm and an outer diameter of 812.8 mm. The pipe length for simulation was set to 2 meters. Defects were odelled as elliptical with varying depths and aspect ratios to examine their influence on stress concentration and corrosion behavior. The mesh was triangular, consisting of 9240 elements with element sizes ranging from 0.1 mm to 5 mm.

3.2. Mechanical Stress Simulation

Mechanical stress analysis was performed using the Solid Mechanics module in COMSOL. The simulation assumed isotropic hardening behavior for the steel, incorporating an experimental stress-strain relationship to model both elastic and plastic deformation regions. A uniform internal pressure of 15 Mpa was applied along the inner surface of the pipe, while longitudinal tensile strains were imposed on one end of the pipe, with the other end fixed. The boundary conditions ensured mechanical equilibrium across the entire model. Von Mises stress was calculated to evaluate stress distribution and its correlation with defect geometry.

3.3. Electrochemical Corrosion Parameters

The electrochemical behavior of the pipeline steel was modelled using the Secondary Current Distribution module. Anodic and cathodic reactions were defined as iron dissolution and hydrogen evolution, respectively. The initial electrochemical parameters, including corrosion potential, current density, and Tafel slopes, were derived from polarization curves reported in the literature. These parameters were consistent with those employed by [3], who demonstrated the interaction between mechanical deformation and electrochemical behavior in pipelines under near-neutral pH conditions.

The boundary conditions for the solution assumed electrical isolation, except at the steel-solution interface, which was set as an active surface for electrochemical reactions.

4. Finding and Discussion

4.1. Von Mises Stress Distribution

The simulation results reveal significant variations in Von Mises stress distribution across different defect aspect ratios (2:1, 4:1, 6:1, and 8:1) and strain rates. For defects with a 2:1 aspect ratio, the peak Von Mises stress at the defect center ranges from 550 MPa to 853 MPa under displacements of 1 mm to 4 mm, as shown in Figure 1(a) to 1(d). The stress gradients are smooth, with broader stress distributions as displacement increases, indicating less localized deformation.

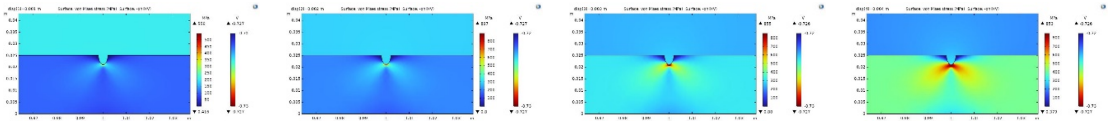

(a) (b) (c) (d)

Figure 1. Von Mises Stress Distribution for a 2:1 Defect Aspect Ratio: (a) 1 (b) 2 (c) 3 (d) 4 mm/s

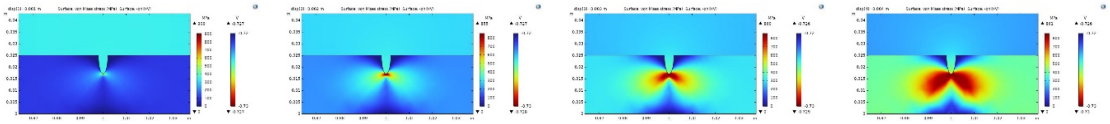

(a) (b) (c) (d)

Figure 2. Von Mises Stress Distribution for a 4:1 Defect Aspect Ratio: (a) 1 (b) 2 (c) 3 (d) 4 mm/s

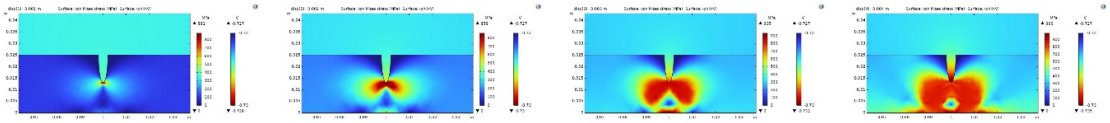

(a) (b) (c) (d)

Figure 3. Von Mises Stress Distribution for a 6:1 Defect Aspect Ratio: (a) 1 (b) 2 (c) 3 (d) 4 mm/s

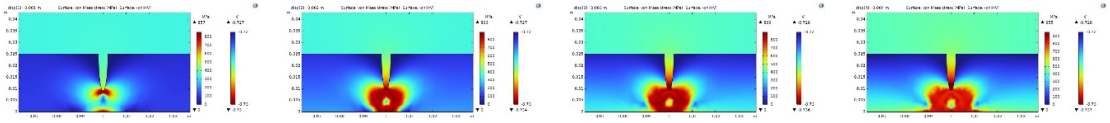

(a) (b) (c) (d)

Figure 4. Von Mises Stress Distribution for an 8:1 Defect Aspect Ratio: (a) 1 (b) 2 (c) 3 (d) 4 mm/s

As the aspect ratio increases to 4:1, the peak Von Mises stress rises significantly, reaching up to 909 MPa at a displacement of 1 mm (Figure 2(a)). However, at higher displacements, the stress stabilizes around 860 MPa to 861 MPa (Figures 2(c) and 2(d)). This behavior reflects a balance between localized stress concentration and redistribution into adjacent areas, as the defect geometry amplifies stress around the center while spreading it across the material.

For defects with a 6:1 aspect ratio, the stress becomes increasingly localized, with peak Von Mises stress values ranging from 881 MPa to 990 MPa under displacements of 1 mm to 4 mm (Figures 3(a) to 3(d)). The stress fields broaden progressively, indicating substantial deformation and stress redistribution into surrounding regions, which aligns with a higher risk of crack initiation and material degradation.

At an 8:1 aspect ratio, the stress concentration becomes most pronounced, with peak values increasing from 857 MPa at 1 mm displacement to 955 MPa at 4 mm displacement (Figures 4(a) to 4(d)). The defect geometry at this ratio causes extreme localization of stress at the defect center, while the surrounding regions experience significant stress redistribution, further exacerbating material weakening.

These findings demonstrate that as the aspect ratio increases, the peak Von Mises stress and the severity of stress concentration amplify significantly. Higher aspect ratios lead to sharper stress gradients and broader redistribution at higher displacements, increasing the risk of failure through crack propagation and localized plastic deformation [30] [31]. The combined effects of defect geometry and displacement emphasize the need for precise monitoring and advanced mitigation strategies to prevent catastrophic pipeline failures under operational loading conditions.

4.2. Influence of Strain Rates on Von Mises Stress

The effect of strain rates on Von Mises stress distribution is illustrated in Figure 5.

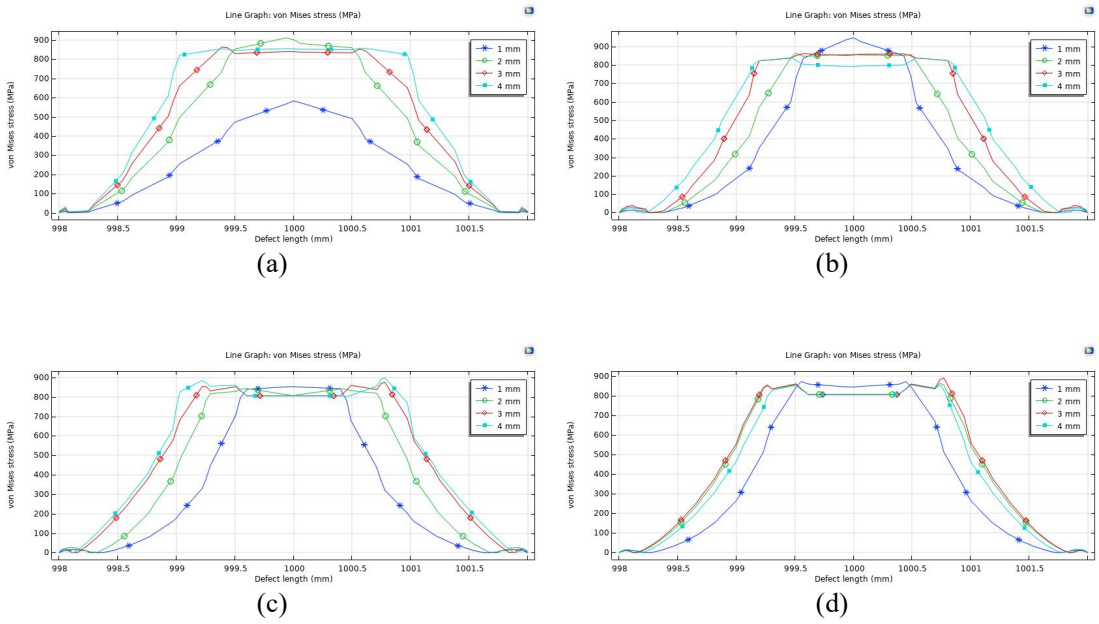

Figure 5. Effect of Strain Rate on Von Mises Stress Distribution for Defect Aspect Ratios: (a) 2:1 (b) 4:1 (c) 6:1 (d) 8:1

For all defect aspect ratios (2:1, 4:1, 6:1, and 8:1), increasing strain rates from 1 mm/s to 4 mm/s results in a notable rise in peak stress values. At the lowest aspect ratio (2:1), the stress distribution remains relatively broad, with peak stress increasing from 550 MPa to 853 MPa. However, as the aspect ratio increases, stress concentration becomes more pronounced. For the 4:1 aspect ratio, the peak stress ranges from 860 MPa to 909 MPa, with steeper gradients around the defect. For higher aspect ratios like 6:1 and 8:1, the stress distribution narrows significantly, with peak values reaching 990 MPa and 955 MPa, respectively, at 4 mm/s, reflecting severe localization near the defect center.

The findings highlight a strong dependency of stress concentration on strain rates, especially for defects with sharper geometries. Higher strain rates exacerbate stress localization due to the increased rate of energy transfer and deformation [32] [33]. This trend is particularly evident in higher aspect ratios, where stress gradients are sharper, and redistribution is minimal, amplifying the likelihood of localized failure [34]. These results suggest that operational strain rates need to be carefully managed in pipeline systems, as elevated strain rates significantly increase the mechanical vulnerability of defects, particularly those with high aspect ratios.

4.3. Long-Term Stress Redistribution Due to Material Degradation

The long-term effects of material degradation on Von Mises stress distribution are shown in Figure 6. For the 2:1 aspect ratio, stress is relatively uniform at 0 years, with a peak value of approximately 860 MPa. After 20 years, the peak stress increases to 900 MPa, and the stress field broadens, indicating redistribution into surrounding areas. For the 4:1 aspect ratio, the peak stress rises from 850 MPa to 880 MPa, and the stress field shows further expansion. At higher aspect ratios, such as 6:1 and 8:1, the peak stress remains steady at approximately 900 MPa, but the stress distribution broadens significantly, amplifying stress beyond the defect's immediate vicinity.

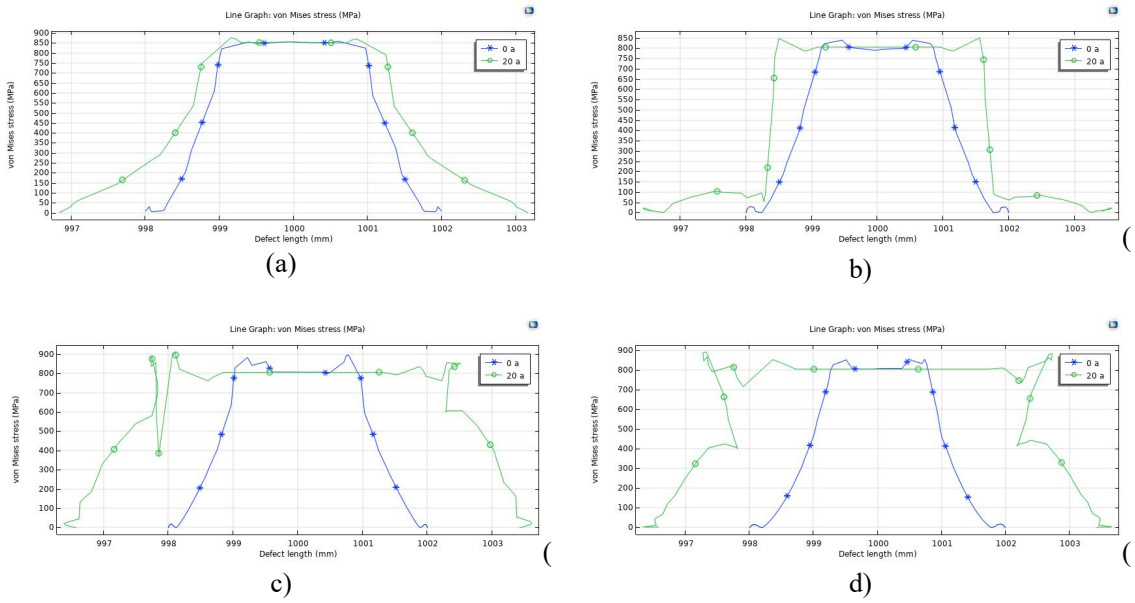

Figure 6. Long-Term Changes in Stress Distribution (0 and 20 years) for Defect Aspect Ratios: (a) 2:1 (b) 4:1 (c) 6:1 (d) 8:1

These results underscore the compounding effects of material aging and defect geometry on stress behavior. Over time, degradation weakens the material around the defect, leading to stress redistribution and an increased likelihood of crack propagation [35]. The broadening of the stress field over 20 years reflects the gradual shift from localized to more distributed stress, which can undermine the structural integrity of the pipeline [36]. For sharp defects (e.g., 6:1 and 8:1), the persistence of high peak stress coupled with broader redistribution poses critical risks for long-term pipeline reliability [37]. This necessitates regular monitoring and maintenance to mitigate the effects of material aging and prevent catastrophic failures.

4.4. Analysis of Anodic and Cathodic Current Density

4.4.1. Anodic Current Density

The simulation results reveal that the anodic current density distribution is highly influenced by the defect geometry and strain rate. For defects with lower aspect ratios (2:1) and shallow depths, the anodic current density at the defect center was relatively uniform, averaging around 3.5 μA/cm² under low strain rates. However, for defects with higher aspect ratios (8:1), the anodic current density increased significantly, exceeding 6 μA/cm² at the defect center under higher strain rates. Contour plots illustrate that higher aspect ratios result in sharper gradients of anodic current density, localized at the defect apex, while the edges of the defect exhibit lower current density values. This distribution indicates that the defect center serves as the primary anodic region, driving localized corrosion activity.

The increased anodic current density at the defect center for high aspect ratio geometries highlights the synergistic effect of stress concentration and electrochemical activity. The sharp stress gradients at the defect center enhance the anodic reaction rates, aligning with the mechanoelectrochemical theory, which posits that mechanical deformation elevates electrochemical activity [38].

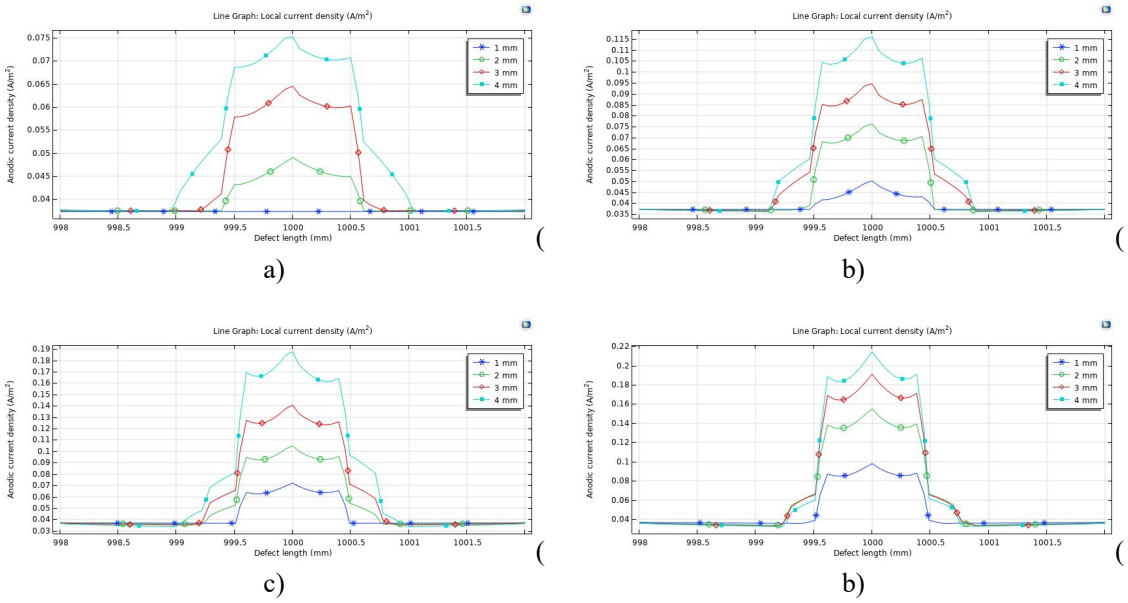

Figure 7. Anodic Current Density Distribution Based on Defect Aspect Ratio: (a) 2:1 (b) 4:1 (c) 6:1 (d) 8:1

The reduced current density at the defect edges suggests that these regions act as cathodic zones, creating a localized galvanic cell that accelerates corrosion at the defect center [39]. This phenomenon underscores the critical role of defect geometry in influencing corrosion rates, where deeper defects with sharp geometries exacerbate material degradation [40]. These insights suggest the necessity for targeted corrosion mitigation strategies, such as optimizing cathodic protection systems, to address regions of elevated anodic current density and prevent localized failure.

4.4.2. Cathodic Current Density

Figure 8 shows the Cathodic Current Density Distribution.

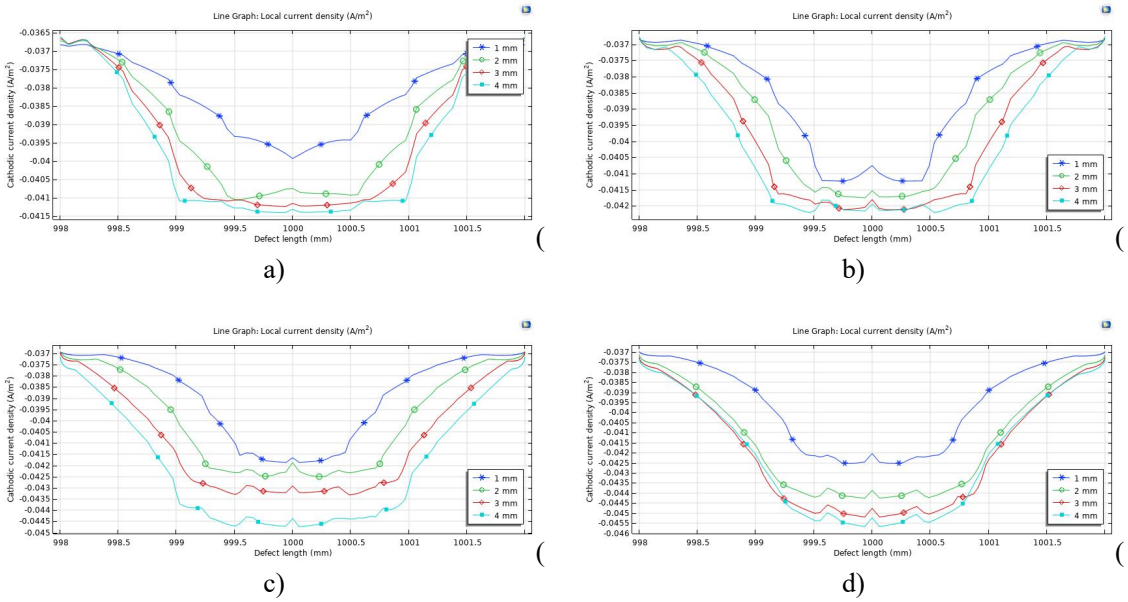

Figure 8. Cathodic Current Density Distribution Based on Defect Aspect Ratio: (a) 2:1 (b) 4:1 (c) 6:1 (d) 8:1

The cathodic current density distribution, primarily associated with hydrogen evolution, shows a distinct variation across different defect geometries and strain rates. For defects with shallow depths and lower aspect ratios (2:1), the cathodic current density remained uniform at approximately -3.5 μA/cm² under low strain rates. In contrast, defects with higher aspect ratios (8:1) exhibited more pronounced cathodic activity, with current density values becoming increasingly negative, reaching -6.5 μA/cm² at the defect center under higher strain rates. Contour plots illustrate that the defect center consistently experiences the most negative cathodic current density, while the defect edges display less negative values, indicative of reduced cathodic activity.

The localized increase in cathodic current density at the defect center corresponds to intensified hydrogen evolution, which is mechanically driven by stress concentration. The elevated negative current density at high aspect ratios suggests a feedback mechanism where localized stress enhances cathodic activity, promoting hydrogen permeation and embrittlement of the surrounding material [41] [42]. This phenomenon reduces the structural integrity of the defect region, exacerbating the likelihood of crack initiation [43].

Furthermore, the contrast between the defect center and edges creates a potential gradient that drives localized corrosion processes [44]. These findings highlight the importance of addressing cathodic activity in defect regions to mitigate hydrogen-induced degradation, emphasizing the need for enhanced cathodic protection designs tailored to defect geometries.

5. Conclusion

This study demonstrated the significant influence of defect geometry and strain rate on the mechanoelectrochemical behavior of X100 steel pipelines. Higher defect aspect ratios and deeper geometries resulted in pronounced Von Mises stress concentrations, exceeding 600 MPa, particularly at the defect center, and were further amplified under higher strain rates, accelerating plastic deformation. The anodic current density increased significantly at the defect center for sharper defects, driving localized corrosion, while the cathodic current density mirrored this behavior with enhanced hydrogen evolution, contributing to hydrogen embrittlement and material degradation. The interplay between mechanical stress and electrochemical reactions highlights the critical role of defect geometry in pipeline integrity, where dynamic loading conditions exacerbate both stress and corrosion activity. These findings emphasize the importance of defect monitoring, advanced material designs, and optimized cathodic protection systems to enhance the safety and longevity of pipelines. Future research needs to examine the impacts of long-term cyclic loading and environmental factors, including temperature and pressure variations, to enhance predictive models and mitigation strategies for pipeline degradation.

References

[1] Q. Ma, “Microstructure Design and Properties of X100 Gas Line Pipe,” in *IOP Conference Series: Earth and Environmental Science*, 2020.

[2] X. Ye *et al.*, “Microstructure Characterization and Strengthening Mechanism Analysis of X100 Pipeline Steel,” *Coatings*, vol. 13, no. 4, 2023.

[3] L. Xu, “Assessment of corrosion defects on high-strength steel pipelines,” (Doctoral Thesis), University of Calgary, Canada, 2013.

[4] Z. Liang, Y. Xiao, and J. Zhang, “Stress-Strain Analysis of a Pipeline With Inner and Outer Corrosion Defects,” *J. Press. Vessel Technol. Trans. ASME*, vol. 140, no. 6, 2018.

[5] Z. Zhang, X. Ni, and Y. Frank Cheng, “Assessment by finite element modelling of the mechano-electrochemical interaction at double-ellipsoidal corrosion defect with varied inclinations on pipelines,” *Constr. Build. Mater.*, vol. 260, p. 120459, 2020.

[6] K. F. Tee and A. H. Wordu, “Burst strength analysis of pressurized steel pipelines with corrosion and gouge defects,” *Eng. Fail. Anal.*, vol. 108, no. July 2019, p. 104347, 2020.

[7] Y. Wang, L. Xu, J. Sun, and Y. F. Cheng, “Mechano-electrochemical interaction for pipeline corrosion: A review,” *J. Pipeline Sci. Eng.*, vol. 1, no. 1, pp. 1–16, 2021.

[8] G. Mubarak, I. Gadala, I. Barsoum, and A. Alfantazi, “Numerical investigation of the mechano-electro-chemical effect of X100 buried pipelines with pre-existing corrosion defects,” *Heliyon*, vol. 9, no. 12, p. e22440, 2023.

[9] S. . Sushmitha Evangeliene, D. . Robinson Smart, V. Saravanan, and M. Ramachandran, “An

Overview High Performance of Stress Corrosion Cracking Behavior for Aeronautic Applications," *J. Mater. its Charact.*, vol. 2, no. 2, pp. 9–19, 2023.

[10] S. A. Abubakar, S. Mori, and J. Sumner, "Effect of Dissolved CO2 on the Interaction of Stress and Corrosion for Pipeline Carbon Steels in Simulated Marine Environments," *Metals (Basel).*, vol. 13, no. 7, 2023.

[11] M. Yadav, M. H. Sliem, A. M. Abdullah, K. M. Youssef, and N. H. Al-Qahtani, "Impact of Prolonged Exposure to Sour Service on the Mechanical Properties and Corrosion Mechanism of NACE Carbon Steel Material Used in Wet Sour Gas Multiphase Pipeline," *Sustainability*, vol. 14, no. 13, p. 8015, Jun. 2022.

[12] L. Yin, M. Li, W. Sun, J. Chen, B. Liu, and Z. Wang, "Mechanical Mechanism and Propagation Law of Fissure-Tip Cracks of Large-Size Rock Specimens with Two Precut Fissures," *Shock Vib.*, vol. 2021, no. 1, Jan. 2021.

[13] P. Seenuan, N. Noraphaiphipaksa, and C. Kanchanomai, "Stress Intensity Factors for Pressurized Pipes with an Internal Crack: The Prediction Model Based on an Artificial Neural Network," *Appl. Sci.*, vol. 13, no. 20, p. 11446, Oct. 2023.

[14] C. Qi and A. Pi, "An experimental calculation method for stress intensity factors of three-dimensional surface cracks," *J. Mech.*, vol. 40, pp. 654–664, Jan. 2024.

[15] M. Janssen, J. Zuidema, and R. J. H. Wanhill, *Fracture Mechanics: An Engineering Primer*. TU Delft OPEN Publishing, 2024.

[16] N. Sommer, I. Kryukov, C. Wolf, M. Wiegand, M. Kahlmeyer, and S. Böhm, "On the Intergranular Corrosion Properties of Thin Ferritic Stainless Steel Sheets Welded by Fiber-Laser," *Metals (Basel).*, vol. 10, no. 8, p. 1088, Aug. 2020.

[17] S. Xu, H. Zhang, B. Nie, and Z. Zhang, "Effect of Pitting Corrosion on the Stress Intensity Factor Magnitude and Distribution," *Int. J. Steel Struct.*, vol. 21, no. 4, pp. 1454–1464, Aug. 2021.

[18] F. Brownlie, T. Hodgkiess, A. Pearson, and A. M. Galloway, "Erosion-Corrosion Mechanisms of Engineering Steels in Different NaCl Concentrations," *J. Bio- Tribo-Corrosion*, vol. 7, no. 2, p. 80, Jun. 2021.

[19] T. O. Olugbade, "Electrochemical Characterization of the Corrosion of Mild Steel in Saline Following Mechanical Deformation," *Anal. Lett.*, vol. 54, no. 6, pp. 1–13, 2020.

[20] University of Cambridge, "The Tafel Plot," 2020. [Online]. Available: https://www.doitpoms.ac.uk/tlplib/aqueous_corrosion/tafel_plot.php. [Accessed: Dec 2024]

[21] D. Sobola and R. Dallaev, "Exploring Hydrogen Embrittlement: Mechanisms, Consequences, and Advances in Metal Science," *Energies*, vol. 17, no. 12, p. 2972, Jun. 2024.

[22] X. Li, X. Ma, J. Zhang, E. Akiyama, Y. Wang, and X. Song, "Review of Hydrogen Embrittlement in Metals: Hydrogen Diffusion, Hydrogen Characterization, Hydrogen Embrittlement Mechanism and Prevention," *Acta Metall. Sin. (English Lett.*, vol. 33, no. 6, pp. 759–773, Jun. 2020.

[23] U. Sarwar *et al.*, "Enhancing pipeline integrity: a comprehensive review of deep learning-enabled finite element analysis for stress corrosion cracking prediction," *Eng. Appl. Comput. Fluid Mech.*, vol. 18, no. 1, Dec. 2024.

[24] H. Zhao, X. Liang, Z. Yang, P. He, and B. Zhao, "Experimental and Numerical Analysis of the Impact of Corrosion on the Failure Pressure of API 5L X65 Pipeline," *J. Mar. Sci. Eng.*, vol. 12, no. 10, p. 1810, Oct. 2024.

[25] A. Ali, D. I. Permana, and H. N. Yudha, "Analysis of variance dimension of reinforcement to stress concentration factor using Finite Element Method," *SINERGI*, vol. 26, no. 3, p. 295, Oct. 2022.

[26] A. Meroufel, A. Gordon, and D. Thierry, "Cathodic protection shielding of coated buried pipeline," *J. Coatings Technol. Res.*, vol. 21, no. 2, pp. 445–459, Mar. 2024.

[27] W. Zhang, X. Wang, H. Li, Z. Lin, and Z. Chen, "The Influence of Rust Layers on Calcareous Deposits' Performance and Protection Current Density in the Cathodic Protection Process," *Coatings*, vol. 14, no. 8, p. 1015, Aug. 2024.

[28] S. Yamada and Y. Jiao, "Damage Evaluation Method for Steel Beams Subjected to Cyclic Loading," *Int. J. Steel Struct.*, vol. 22, no. 6, pp. 1850–1863, Dec. 2022.

[29] M. Wasim and M. B. Djukic, "External corrosion of oil and gas pipelines: A review of failure mechanisms and predictive preventions," *J. Nat. Gas Sci. Eng.*, vol. 100, p. 104467, Apr. 2022.

[30] S. S. Shishvan, S. Assadpour-asl, and E. Martínez-Pañeda, "A mechanism-based gradient damage model for metallic fracture," *Eng. Fract. Mech.*, vol. 255, 2021.

[31] D. Zhao, B. Yin, and M. Kaliske, "Concrete failure based on a localizing gradient-enhanced damage formulation coupled with plasticity," *PAMM*, vol. 23, no. 2, pp. 1–7, 2023.

[32] B. Dalai, M. A. Moretti, P. Åkerström, V. A. Esin, and L. E. Lindgren, "Mechanical behavior and microstructure evolution during high strain rate deformation of AA7075-T651," *SN Appl. Sci.*, vol. 4, no. 10, 2022.

[33] F. Tetteh, S. Duntu, and S. Boakye-Yiadom, "Multiscale Evolution of Strain Localisation Mechanisms in AZ31B Magnesium and 7050 Aluminum Alloys at High Strain Rates," *Microsc. Microanal.*, vol. 26, no. S2, pp. 1078–1080, 2020.

[34] Y. Z. Jia, H. Li, N. N. Hu, Q. Y. Wang, and J. Q. Wang, "Comparative assessment of near-neutral pH stress corrosion cracking resistance of pipeline steels with different strength," *Mater. Corros.*, vol. 66, no. 11, pp. 1250–1254, 2015.

[35] C. Guerre, M. Frégonèse, Q. Auzoux, I. Aubert, and C. Duhamel, "Stress corrosion crack propagation," in *Mechanics - Microstructure - Corrosion Coupling: Concepts, Experiments, Modeling and Cases*, pp. 313–338, 2019.

[36] H. Shirazi, S. Wang, R. Eadie, and W. Chen, "Pipeline Circumferential Cracking in Near-Neutral pH Environment Under the Influence of Residual Stress: Dormancy and Crack Initiation," *Metall. Mater. Trans. A Phys. Metall. Mater. Sci.*, vol. 55, no. 9, pp. 3640–3661, 2024.

[37] G. Qin and Y. F. Cheng, "Modeling of mechano-electrochemical interaction at a corrosion defect on a suspended gas pipeline and the failure pressure prediction," *Thin-Walled Struct.*, vol. 160, no. June 2020, p. 107404, 2021.

[38] S. R. Shah, L. S. De Vasconcelos, and K. Zhao, "Computational Modeling of Electrochemomechanics of High-Capacity Composite Electrodes in Li-Ion Batteries," *J. Appl. Mech. Trans. ASME*, vol. 89, no. 8, pp. 32–39, 2022.

[39] D. Filotás, J. Izquierdo, B. M. Fernández-Pérez, L. Nagy, G. Nagy, and R. M. Souto, "Contributions of Microelectrochemical Scanning Techniques for the Efficient Detection of Localized Corrosion Processes at the Cut Edges of Polymer-Coated Galvanized Steel," *Molecules*, vol. 27, no. 7, 2022.

[40] S. D. Vijaya Kumar, S. Karuppanan, V. Perumal, and M. Ovinis, "Failure pressure prediction of high-strength steel pipe bend considering pipe and corrosion geometry," *Discov. Appl. Sci.*, vol. 6, no. 4, 2024.

[41] H. Wan *et al.*, "Effect of negative half-wave alternating current on stress corrosion cracking behavior and mechanism of X80 pipeline steel in near-neutral solution," *Constr. Build. Mater.*, vol. 154, pp. 580–589, 2017.

[42] Y. Pan, Z. Liu, Y. Zhang, X. Li, and C. Du, "Effect of AC Current Density on the Stress Corrosion Cracking Behavior and Mechanism of E690 High-Strength Steel in Simulated Seawater," *J. Mater. Eng. Perform.*, vol. 28, no. 11, pp. 6931–6941, 2019.

[43] A. Mohammadi, M. Koyama, G. Gerstein, H. J. Maier, and H. Noguchi, "Hydrogen-assisted crack propagation in pre-strained twinning-induced plasticity steel: From initiation at a small defect to failure," *ISIJ Int.*, vol. 61, no. 4, pp. 1278–1286, 2021.

[44] C. Xie, S. Bai, X. Liu, M. Zhang, and J. Du, "Stress-corrosion coupled damage localization induced by secondary phases in bio-degradable Mg alloys: phase-field modeling," *J. Magnes. Alloy.*, vol. 12, no. 1, pp. 361–383, 2024.